8304 *Inorg. Chem.* **2009**, *48*, 8304–8316
DOI: 10.1021/ic9009459

Inorganic Chemistry
Article

Synthesis and Characterization of Alkali-Metal Salts of 2,2′- and 2,4′-Bipyridyl Radicals and Dianions

Edward Gore-Randall, Mark Irwin, Mark S. Denning, and Jose M. Goicoechea*

Chemistry Research Laboratory, Department of Chemistry, University of Oxford, Mansfield Road, Oxford OX1 3TA, U.K.

Received May 14, 2009

The reaction of ethylenediamine (en) solutions of 2,2′- and 2,4′-bipyridine (bipy) with varying stoichiometric amounts of potassium and rubidium metal resulted in the isolation of compositionally pure solids containing the respective bipyridyl radical anions (2,2′- and 2,4′-bipy$^{\bullet-}$) and dianions (2,2′- and 2,4′-bipy^{2-}). These species were structurally characterized by single-crystal X-ray diffraction in K(2,2′-bipy)(en) (**1a**), K_4(2,2′-bipy)$_4$(en)$_4$ (**1b**), Rb_2(2,2′-bipy)(en)$_2$ (**2**), K(2,4′-bipy)(en) (**3**), K_4(2,4′-bipy)$_2$(en)$_{3.5}$ (**4**), and Rb_4(2,4′-bipy)$_2$(en)$_{3.5}$ (**5**). The crystallographic results obtained allow for interesting relationships to be drawn between the electronic structure of the bipyridyl moieties and metric structural data. Further characterization of the solids by means of powder X-ray diffraction, elemental analysis, electron paramagnetic resonance, and IR and Raman spectroscopy is also reported. These studies provide a comprehensive overview of the structural and spectroscopic properties of these often-cited yet elusive air- and moisture-sensitive species, helping to complement the existing data in the chemical literature.

1. Introduction

Of the three most readily available structural isomers of bipyridine (bipy), the 2,2′ isomer is by far the most extensively studied because of its ability to chelate metal centers.[1] As a result, 2,2′-bipy has been ubiquitously employed in coordination chemistry, and a wealth of information is available in the chemical literature regarding the electrochemical behavior and spectroscopic properties of the ligand itself and of the coordination complexes it forms. Similarly, 4,4′-bipy has also been extensively investigated because of its widespread use as a linear linker in coordination polymers and metal−organic frameworks.[2] Finally, the 2,4′ isomer is perhaps the least studied of the three because of its inability to act as either a bidentate chelate or an effective bridging spacer between metal atoms. The three remaining isomers, 2,3′, 3,3′, and 3,4′, are seldom employed in coordination chemistry, and there is little information available in the literature regarding their spectroscopic properties and reactivity despite the fact that the two former isomers are the only known naturally occurring forms of bipyridine.[3] The relative "popularity" of an isomer is similarly reflected in the amount of structural data available for each species. A survey of crystallographically characterized compounds using the CCDC structural database shows that while there are 5218 single-crystal X-ray structures containing 2,2′-bipy, there are 3127 for the 4,4′ isomer and a mere 44 for the 2,4′ isomer (a search for the 2,3′, 3,3′, and 3,4′ isomers yields 2, 19, and 3 hits, respectively).[4] These numbers do not include functionalized bipyridyl-based systems, of which there are many more examples in the chemical literature, particularly for species containing the 2,2′-bipy moiety.[5]

These observations are also manifested in the information available on the chemically reduced forms of the isomers. It has long been established that the chemical reduction of 2,2′-bipy can give rise to the 2,2′-bipyridyl radical anion.[6] A further reduction of the radical species is also known to yield the 2,2′-bipyridyl dianion, which relatively recently was crystallographically characterized as an alkali-metal salt

*To whom correspondence should be addressed. E-mail: jose.goicoechea@chem.ox.ac.uk.

(1) Reedijk, J. Heterocyclic Nitrogen-donor Ligands. In *Comprehensive Coordination Chemistry: The Synthesis, Reactions, Properties and Applications of Coordination Compounds*; Wilkinson, G., Gillard, R. D., McCleverty, J. A., Eds.; Pergamon Press: Oxford, U.K., 1987; Vol. *2*, Chapter 13.2.

(2) (a) Stang, P. J. *Chem.—Eur. J.* **1998**, *4*, 19. (b) Olenyuk, B.; Fechtenkötter, A.; Stang, P. J. *J. Chem. Soc., Dalton Trans.* **1998**, 1707. (c) Jones, C. J. *Chem. Soc. Rev.* **1998**, *27*, 289. (d) Yaghi, O. M.; Li, H.; Davis, C.; Richardson, D.; Groy, T. L. *Acc. Chem. Res.* **1998**, *31*, 474. (e) Kitagawa, S.; Kitaura, R.; Noro, S. *Angew. Chem., Int. Ed.* **2004**, *43*, 2334. (f) James, S. L. *Chem. Soc. Rev.* **2003**, *32*, 276.

(3) (a) Schumacher, J. N.; Green, C. R.; Best, F. W.; Newell, M. P. *J. Agric. Food Chem.* **1977**, *25*, 310. (b) Foder, G. B.; Colasanti, B. In *Alkaloids: Chemical and Biological Perspectives*; Pelletier, S. W., Ed.; Wiley: New York, 1985; Vol. *3*, Chapter 1.

(4) Numbers according to CSD, version 5.30 (Nov **2008**).

(5) (a) Smith, A. P.; Fraser, C. L. Bipyridine Ligands. In *Comprehensive Coordination Chemistry II: From Biology to Nanotechnology*, 2nd ed.; Lever, A. B. P., McCleverty, J. A., Meyer, T. J., Eds.; Elsevier: New York, 2005; Vol. *1*, Chapter 1.1. (b) Kaes, C.; Katz, A.; Hosseini, M. W. *Chem. Rev.* **2000**, *100*, 3553.

(6) For reviews on this topic, see: (a) Creutz, C. *Comments Inorg. Chem.* **1982**, *1*, 293. (b) Kaim, W. *Coord. Chem. Rev.* **1987**, *76*, 187.

Published on Web 08/12/2009

and in a lanthanide coordination complex.[7,8] Extensive IR,[9] Raman,[10] UV−vis,[11] and electron paramagnetic resonance (EPR)[12] spectroscopic data are available for the radical-anionic form of 2,2′-bipy (2,2′-bipy$^{\bullet-}$) in saltlike species and in coordination compounds. Similarly, electrochemical data for the 2,2′- and 4,4′-bipy isomers have also been previously reported in the literature.[13] However, an in-depth analysis of the spectroscopic data available often reveals contradictory reports, perhaps because of the difficulty associated with the isolation of these highly air- and moisture-sensitive species and with the bulk characterization of the samples. Furthermore, despite the relatively well-established nature of these highly reduced species, structural data are extremely rare, particularly for "charge-separated" species. As a result, while the single-crystal X-ray structure of an alkali-metal salt of the 2,2′-bipyridyl dianion has been reported,[7] no such data exist for the radical anion. X-ray structures for lanthanide coordination complexes of 2,2′-bipy, in which the coordinated ligand is formally assigned to exist as a radical anion, are well-known.[14] Research carried out by Andersen and co-workers strongly supports such an assignment in species such as $(Cp^*)_2Yb(2,2'\text{-bipy})$ ($Cp^* = C_5(CH_3)_5^-$) by coupling structural data with crucial magnetic susceptibility studies.[15] Furthermore, at least two transition-metal complexes have also been reported in the literature, where bond metric data seem to indicate that these species could be formally discussed as complexes of a 2,2-bipyridyl radical anion; however, in such cases, strong deviations in bond distances from those of neutral bipyridine were argued as evidence of extensive π-back-bonding to a π^* orbital on the ligand.[16]

It is worth noting that the wealth of information available in the chemical literature on chemically reduced forms of 2,2′-bipy is in stark contrast with the lack of information on other isomers, such as 2,4′-bipyridine.[17] Because of the incomplete nature of the structural and spectroscopic data available on reduced forms of 2,2′- and 2,4′-bipy, we set out to isolate and characterize a family of alkali-metal salts of the radical anions and dianions of these bipyridyl isomers. Building on recent work published by our research group detailing the isolation and structural characterization of the 4,4′-bipyridyl radical anion and dianion,[18] we set out to employ similar methodologies to study other structural isomers of bipyridine and build up a database of bond metric and spectroscopic data on the reduced forms of such familiar ligand systems, the results of which are reported herein. We demonstrate that bond distances of the reduced forms of the bipyridyl ligands can be largely used to quantify the charge associated with such species and provide spectroscopic data that complement existing reports in the chemical literature.

2. Experimental Section

Because of the highly air- and moisture-sensitive nature of the products, all reactions and product manipulations were carried out under an inert atmosphere using standard Schlenk-line or glovebox techniques (MBraun UNIlab glovebox maintained at < 0.1 ppm H_2O and < 0.1 ppm O_2). Prior to use, all solvents (diethyl ether, 99.9%, Rathburn; toluene, 99.9%, Rathburn) were dried using an MBraun MB SPS-800 solvent purification system. Ethylenediamine (en; 99.9%, Rathburn) was purified by distillation over sodium metal. All solvents were stored in gas-tight ampules under argon. Toluene and diethyl ether were stored over activated 3 Å molecular sieves (Acros). Potassium (99.95%, Aldrich) and rubidium (99.9 + %, Strem) were used as delivered and stored in the glovebox. 2,2′-Bipyridine (2,2′-bipy; > 99%, TCI Europe) and 2,4′-bipyridine (2,4′-bipy; > 99%, TCI Europe) were used as delivered after careful drying of the solids under vacuum.

K(2,2′-bipy)(en) (1). 2,2′-bipy (0.144 g, 0.92 mmol) and potassium metal (0.038 g, 0.97 mmol) were dissolved in approximately 4 mL of en, instantly yielding a deep-purple solution. The reaction mixture was stirred for approximately 24 h in a capped sample vial in a nitrogen-filled glovebox. The solution was filtered into a crystallization ampule while in the glovebox by passing it through a Pasteur pipette containing packed glass wool at the constriction. Prior to use, an ampule containing the glass-wool-packed pipette was heated under vacuum to drive off all traces of moisture and air. After filtration, the sealed ampule was transferred to a Schlenk line, where it was layered with toluene (approximately 20 mL). During layering, the ampule was cooled in a water bath (8 °C) and then transferred to a fridge (8−10 °C) to aid the crystallization of the product. Two polymorphic crystalline products formed after 4 days: K(2,2′-bipy)(en) (**1a**) and $K_4(2,2'\text{-bipy})_4(en)_4$ (**1b**). Both crystallized as large purple/black blocklike crystals and were found to be suitable for single-crystal X-ray diffraction. Crystalline yield: 39.8%. Anal. Calcd for $C_{12}H_{16}N_4K$: C, 56.42; H, 6.32; N, 21.95. Found: C, 56.62; H, 6.40; N, 21.86. Solid-state EPR measurements recorded a g value of 2.0033. Solution EPR measurements recorded a g value of 2.0035. IR (cm^{-1}): 626 (m), 683 (s), 709 (s), 738 (w), 817 (w) 939 (s), 974 (s), 1005 (s), 1139 (m), 1155 (m), 1260 (s), 1282 (w), 1404 (m), 1495 (m), 1561 (w). Raman (cm^{-1}): 343 (m), 626 (w), 972 (m), 1020 (w), 1029 (w), 1142 (w), 1157 (s), 1208 (w), 1259 (w), 1347 (m), 1461 (s), 1471 (m), 1495 (m), 1560 (w).

(7) Bock, H.; Lehn, J.-M.; Pauls, J.; Holl, S.; Krenzel, V. *Angew. Chem., Int. Ed.* **1999**, *38*, 952.
(8) Fedushkin, I. L.; Petrovskaya, T. V.; Girgsdies, F.; Köhn, R. D.; Bochkarev, M. N.; Schumann, H. *Angew. Chem., Int. Ed.* **1999**, *38*, 2262.
(9) Saito, Y.; Takemoto, J.; Hutchinson, B.; Nakamoto, K. *Inorg. Chem.* **1972**, *11*, 2003.
(10) (a) Kawashima, H.; Kato, T.; Shida, T. *J. Raman Spectrosc.* **1991**, *22*, 187. (b) Castellà-Ventura, M.; Kassab, E.; Buntinx, G.; Poizat, O. *Phys. Chem. Chem. Phys.* **2000**, *2*, 4682. (c) Danzer, G. D.; Golus, J. A.; Strommen, D. P.; Kincaid, J. R. *J. Raman Spectrosc.* **1990**, *21*, 3. (d) Bradley, P. G.; Kress, N.; Hornberger, B. A.; Dallinger, R. F.; Woodruff, W. H. *J. Am. Chem. Soc.* **1981**, *103*, 7441.
(11) (a) König, E.; Herzog, S. *J. Inorg. Nucl. Chem.* **1970**, *32*, 585. (b) König, E.; Kremer, S. *Chem. Phys. Lett.* **1970**, *5*, 87. (c) Mahon, C.; Reynolds, W. L. *Inorg. Chem.* **1967**, *6*, 1927.
(12) (a) Zahlan, A.; Heineken, F. W.; Bruin, M.; Bruin, F. *J. Chem. Phys.* **1962**, *37*, 683. (b) Dos Santos-Veiga, J.; Reynolds, W. L.; Bolton, J. R. *J. Chem. Phys.* **1966**, *44*, 2214. (c) Henning, J. C. M. *J. Chem. Phys.* **1966**, *44*, 2139. (d) Van Voorst, J. D. W.; Zijlstra, W. G.; Sitters, R. *Chem. Phys. Lett.* **1967**, *1*, 321. (e) König, E.; Fischer, H. *Z. Naturforsch.* **1962**, *17a*, 1063. (f) Kaim, W. *Chem. Ber.* **1981**, *114*, 3789.
(13) (a) Brown, O. R.; Butterfield, R. J. *Electrochim. Acta* **1982**, *27*, 321. (b) Tokel-Takvoryan, N. E.; Hemingway, R. E.; Bard, A. J. *J. Am. Chem. Soc.* **1973**, *95*, 6582.
(14) Evans, W. J.; Gonzales, S. L.; Ziller, J. W. *J. Am. Chem. Soc.* **1994**, *116*, 2600.
(15) (a) Schultz, M.; Boncella, J. M.; Berg, D. J.; Tilley, T. D.; Andersen, R. A. *Organometallics* **2002**, *21*, 460. (b) Walter, M. D.; Berg, D. J.; Andersen, R. A. *Organometallics* **2006**, *25*, 3228. (c) Booth, C. H.; Walter, M. D.; Kazhdan, D.; Hu, Y.-J.; Lukens, W. W.; Bauer, E. D.; Maron, L.; Eisenstein, O.; Andersen, R. A. *J. Am. Chem. Soc.* **2009**, *131*, 6480.
(16) (a) Chisholm, M. H.; Huffman, J. C.; Rothwell, I. P.; Bradley, P. G.; Kress, N.; Woodruff, W. H. *J. Am. Chem. Soc.* **1981**, *103*, 4945. (b) Radonovich, L. J.; Eyring, M. W.; Groshens, T. J.; Klabunde, K. J. *J. Am. Chem. Soc.* **1982**, *104*, 2816.
(17) (a) Yang, L.; Wimmer, F. L.; Wimmer, S.; Zhao, J.; Braterman, P. S. *J. Organomet. Chem.* **1996**, *525*, 1. (b) Oe, S.; Fukushima, K. *J. Mol. Struct.* **1990**, *223*, 337.
(18) Denning, M. S.; Irwin, M.; Goicoechea, J. M. *Inorg. Chem.* **2008**, *47*, 6118.

$Rb_2(2,2'\text{-bipy})(en)_2$ (2). Sample **2** was prepared by the same method as that employed for the synthesis of **1** using 2,2′-bipy (0.192 g, 1.23 mmol) and rubidium metal (0.221 g, 2.58 mmol). Purple/black rodlike crystals of **2** suitable for single-crystal X-ray diffraction were isolated from an en/toluene mixture (crystalline yield: 35.0%). Powder X-ray diffraction studies found that the bulk sample matched the calculated diffraction pattern, as predicted from single-crystal data. Anal. Calcd for $C_{14}H_{24}N_6Rb_2$: C, 37.57; H, 5.41; N, 18.79. Found: C, 37.56; H, 5.51; N, 18.70. Solid-state EPR measurements recorded a weak resonance with a *g* value of 2.0033. IR (cm^{-1}): 612 (vs), 639 (m), 668 (s), 675 (s), 708 (w), 755 (m), 801 (s), 830 (m), 867 (m), 887 (s), 902 (m), 928 (w), 980 (s), 1018 (m), 1039 (vs), 1090 (s), 1099 (s), 1149 (w), 1260 (s), 1290 (m), 1322 (w), 1363 (m), 1399 (s), 1560 (m), 1590 (m). Raman (cm^{-1}): 327 (w), 433 (m), 464 (w), 589 (w), 607 (w), 642 (w), 709 (m), 916 (m), 957 (s), 989 (s), 1083 (s), 1108 (w), 1137 (m), 1154 (w), 1233 (s), 1303 (m), 1345 (w), 1434 (s), 1469 (m), 1493 (s), 1578 (s).

K(2,4′-bipy)(en) (3). Sample **3** was prepared by the same method as that employed for the synthesis of **1** using 2,4′-bipy (0.152 g, 0.97 mmol) and potassium metal (0.040 g, 1.02 mmol). Dark-purple/black platelike crystals of **3** suitable for single-crystal X-ray diffraction were isolated from an en/toluene mixture after 4 days (crystalline yield: 11.7%). Powder X-ray diffraction studies found that the bulk sample matched the calculated diffraction pattern, as predicted from single-crystal data. Anal. Calcd for $C_{12}H_{16}N_4K$: C, 56.42; H, 6.32; N, 21.95. Found: C, 56.36; H, 6.27; N, 21.86. Solid-state and solution-phase EPR measurements recorded a *g* value of 2.0037. IR (cm^{-1}): 625 (w), 668 (w), 689 (m), 739 (m), 745 (m), 772 (w), 793 (m), 932 (m), 944 (s), 960 (w), 978 (m), 1016 (m), 1144 (s), 1202 (s), 1252 (m), 1267 (w), 1303 (w), 1426 (s), 1559 (s), 1586 (s), 1597 (s). Raman (cm^{-1}): 335 (m), 429 (w), 590 (w), 598 (w), 741 (w), 982 (m), 1012 (s), 1028 (w), 1040 (m), 1087 (w), 1149 (m), 1204 (m), 1226 (m), 1260 (w), 1304 (w), 1348 (s), 1406 (w), 1427 (s), 1476 (s), 1504 (s), 1572 (m), 1597 (s).

$K_4(2,4'\text{-bipy})_2(en)_{3.5}$ (4). Sample **4** was prepared by the same method as that employed for the synthesis of **1** using 2,4′-bipy (0.149 g, 0.95 mmol) and potassium metal (0.078 g, 2.00 mmol). Dark-purple/black needlelike crystals formed from an en/toluene mixture after 4 days. Crystalline yield: 81.4%. Anal. Calcd for $C_{27}H_{44}N_{11}K_4$: C, 47.73; H, 6.53; N, 22.69. Found: C, 47.62; H, 6.51; N, 22.66. Solid-state EPR measurements recorded a weak resonance with a *g* value of 2.0035. IR (cm^{-1}): 620 (w), 636 (s), 671 (w), 700 (w), 710 (m), 733 (m), 748 (m), 799 (s), 819 (w), 875 (m), 900 (s), 950 (vs), 981 (m), 1018 (m), 1050 (w), 1072 (m), 1114 (s), 1171 (s), 1208 (s), 1257 (vs, sh), 1290 (vs), 1366 (m), 1410 (w), 1433 (s), 1483 (m), 1502 (m), 1574 (s), 1607 (m). Raman (cm^{-1}): 331 (m), 407 (w), 566 (w), 712 (w), 953 (w), 981 (s), 1012 (w), 1025 (w), 1038 (w), 1072 (m), 1127 (m), 1169 (w), 1210 (m), 1226 (w), 1261 (m), 1344 (m), 1372 (w), 1384 (w), 1431 (m), 1446 (w), 1474 (m), 1504 (s), 1576 (w), 1605 (s).

$Rb_4(2,4'\text{-bipy})_2(en)_{3.5}$ (5). Sample **5** was prepared by the same method as that employed for the synthesis of **1** using 2,4′-bipy (0.155 g, 0.99 mmol) and rubidium metal (0.178 g, 2.08 mmol). Purple rodlike crystals suitable for X-ray diffraction formed after 6 days from an en/diethyl ether mixture (crystalline yield: 58.2%). Powder X-ray diffraction studies found that the bulk sample matched the calculated diffraction pattern, as predicted from single-crystal data. Anal. Calcd for $C_{27}H_{44}N_{11}Rb_4$: C, 37.49; H, 5.13; N, 17.82. Found: C, 37.39; H, 5.07; N, 17.83. Solid-state EPR measurements recorded a weak resonance with a *g* value of 2.0038. IR and Raman data for sample **5** were found to be closely related with those recorded for sample **4**. A complete list of the vibrational data is provided in the Supporting Information.

X-ray Diffraction. Single-crystal X-ray diffraction data were collected using an Enraf-Nonius Kappa-CCD diffractometer and a 95 mm CCD area detector with a graphite-monochromated Mo Kα source ($\lambda = 0.710\,73$ Å). Crystals were selected under Paratone-N oil before being mounted on fibers and positioned under a nitrogen stream. Nitrogen-flow temperatures were controlled by an Oxford Cryosystems cryostream. Equivalent reflections were merged and diffraction patterns processed with the *DENZO* and *SCALEPACK* programs.[19] Structures were subsequently solved using direct methods and refined on F^2 using the *SHELXL 97-2* package.[20]

Transmission powder X-ray diffraction patterns were recorded using a Siemens D5000 diffractometer in modified Debye−Scherrer geometry equipped with an MBraun position-sensitive detector. The instrument produced Cu $K\alpha_1$ radiation (1.540 56 Å) using a germanium monochromator and a standard copper source. Data were recorded on samples in flame-sealed capillaries under nitrogen. The capillaries were mounted on a goniometer head and aligned so that rotation occurred along the long central axis of the capillary. During measurement, the capillary was rotated at ∼60 rpm in order to minimize any preferred orientation effects that might occur.

Computational Methods. Unrestricted geometry optimizations were performed on all of the neutral and negatively charged bipyridyl moieties using atomic coordinates as derived from single-crystal X-ray diffraction experiments. Calculations were performed using the *Gaussian03* package, revision D.01, on the University of Oxford's "ORAC" cluster.[21] All density functional theory (DFT) calculations employed the Becke three-parameter hybrid functional with the Lee−Yang−Parr correlation (B3LYP) in conjunction with the 3-21 + G* basis set.[22,23] Isotropic Fermi contact coupling constants were calculated for the optimized geometries of the 2,2′- and 2,4′-bipyridyl radical species. The program *MOLEKEL6* was used to prepare the three-dimensional plots of electron density.[24]

Additional Characterization Techniques. IR data were recorded on solid samples in Nujol mulls. The mulls were made inside an inert-atmosphere glovebox and the KBr plates placed in an air-tight container prior to data collection. Spectra were recorded on a Nicolet Magna-IR 560 spectrometer in absorbance mode (Happ-Genzel FT apodization) with a Ge/CsI beam splitter and a liquid-nitrogen-cooled mercury−cadmium−telluride detector.

Raman spectra were recorded on solid samples under nitrogen in flame-sealed Pyrex capillaries using a Dilor Labram 300. The excitation radiation was produced by a 20 mW helium−neon laser operating at a wavelength of 632.817 nm. Optical density filters could be inserted into the beam to reduce photon flux, decreasing the likelihood that photochemical reactions would take place during the measurement. Typically, measurements were obtained at 0.1% of the full intensity with a counting time of 100 s. Calibration of the spectrometer was performed before each measurement by referencing the 520.7 nm line of a silicon wafer.

EPR spectra were recorded using a Bruker EMX X-band continuous-wave EPR spectrometer. Solid-state spectra were recorded on approximately 2 mg of the sample in flame-sealed quartz capillaries. For solution spectra, en solutions with concentrations of approximately 0.5 mmol dm^{-3} were made and

(19) Otwinowski, Z.; Minor, W. *Processing of X-ray Diffraction Data Collected in Oscillation Mode*; Academic Press: New York, 1997.

(20) (a) Sheldrick, G. M. *Acta Crystallogr.* **1990**, *A46*, 467. (b) Sheldrick, G. M. *SHELX97—Programs for Crystal Structure Analysis*, release 97-2; Institüt für Anorganische Chemie der Universität: Göttingen, Germany, 1998.

(21) *Gaussian03* package: Frisch, M. J.; et al. *Gaussian03*, revision D.01; Gaussian Inc.: Wallingford, CT, 2004.

(22) (a) Becke, A. D. *J. Chem. Phys.* **1993**, *98*, 5648. (b) Lee, C.; Yang, W.; Parr, R. G. *Phys. Rev. B* **1988**, *37*, 785. (c) Miehlich, B.; Savin, A.; Stoll, H.; Preuss, H. *Chem. Phys. Lett.* **1989**, *157*, 200.

(23) (a) Hay, P. J.; Wadt, W. R. *J. Chem. Phys.* **1985**, *82*, 270. (b) Wadt, W. R.; Hay, P. J. *J. Chem. Phys.* **1985**, *82*, 284. (c) Hay, P. J.; Wadt, W. R. *J. Chem. Phys.* **1985**, *82*, 299.

(24) Portmann, S.; Lüthi, H. P. *Chimia* **2000**, *54*, 766.

portions of 1 mL of the solutions placed in an EPR tube sealed with a Young's tap. EPR simulations were calculated with the *EasySpin* program,[25] and fitting to the experimental spectrum was achieved using a nonlinear least-squares fitting with the Newton−Gauss−Levenberg/Marquardt algorithm.

CHN elemental analyses were performed by Stephen Boyer of London Metropolitan University on 5 mg samples submitted under vacuum in flame-sealed Pyrex ampules.

3. Results and Discussion

3.1. 2,2′-Bipyridyl Radical Anion and Dianion. Synthesis and Crystallographic Characterization. The direct reduction of 2,2′-bipy with an alkali metal such as lithium or sodium has long been established as an efficient route toward chemically reduced forms of bipyridine such as A_2(2,2′-bipy) and A(2,2′-bipy), where A = Li, Na.[26,27] Species such as Na(2,2′-bipy) were first generated in situ in solution over 40 years ago and characterized by EPR spectroscopy,[12] revealing the existence of radical anions in solution. However, these studies failed to offer any information as to the structure of such salts. Electrochemical studies of neutral 2,2′-bipy report chemically accessible standard electrode potentials, making reduction with alkali metals a viable synthetic route toward reduced analogues of the neutral ligand.[13] As mentioned earlier, our research group has recently employed this approach to access the 4,4′-bipyridyl radical and dianion, both of which were isolated and crystallographically characterized as en-containing adducts in Na(4,4′-bipy)(en), Na_2(4,4′-bipy)$_2$(en)$_2$, and Na_2(4,4′-bipy)(en)$_2$.[18]

Analogous studies with 2,2′-bipy revealed that the reaction of 1 equiv of potassium metal with 2,2′-bipy in en yields an intensely colored purple solution, from which we were able to isolate dark-purple air- and moisture-sensitive crystals of the 2,2′-bipyridyl radical anion, 2,2′-bipy$^{\bullet-}$. This species crystallizes as two compositionally identical polymorphs, **1a** and **1b** (Figures 1 and 2, respectively), both of which exhibit similar bond metric parameters for the radical anion. Crystallographic data and experimental parameters for these structures are presented in Table 1. Species **1b** appeared to be the predominant crystallographic phase from a visual inspection of the bulk samples obtained whenever the reaction between potassium metal and 2,2′-bipy was carried out, and on numerous occasions we struggled to observe even trace amounts of the **1a** polymorph. However, when the crystals were ground to a powder in order to confirm the bulk composition of sample **1** by powder X-ray diffraction, a loss of crystallinity occurred. This ultimately prevented us from collecting a powder X-ray diffraction pattern. Despite this, confirmation of the composition of the bulk sample was corroborated by elemental analysis.

When analogous reactions employing a larger stoichiometric excess of an alkali metal (2 equiv) were carried out, we found that the 2,2′-bipyridyl dianion could similarly be synthesized and isolated. We have crystallographically characterized this species in **2**, which was isolated as a dark-purple crystalline solid (Table 1) in relatively high crystalline yields. The bulk composition of sample **2** was confirmed by powder X-ray diffraction (see Figure S1 in the Supporting Information) and elemental analysis.

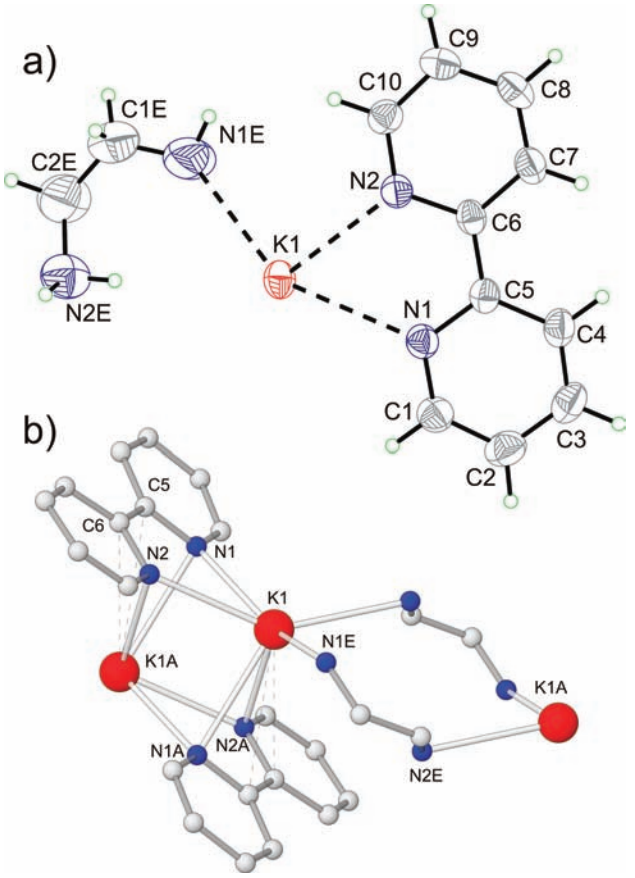

Figure 1. (a) Thermal ellipsoid representation of the atoms in the asymmetric unit of **1a**. Anisotropic displacement ellipsoids pictured at the 50% probability level. (b) Interactions between atoms of the asymmetric unit to build up a one-dimensional chainlike structure. Hydrogen atoms have been omitted for clarity.

Sample **1a** exhibits a single crystallographically unique potassium cation in the asymmetric unit accompanied by a 2,2′-bipyridyl radical anion and an en molecule (Figure 1a). The overall structure can best be described as dimeric units of potassium cations (crystallographically related by symmetry), which are bridged by two 2,2′-bipyridyl radical anions (Figure 1b). These dimers are, in turn, linked together via terminally binding en molecules, giving rise to infinite one-dimensional chains. The chains run parallel to the unit cell *c* axis and pack alongside one another with no apparent interactions between neighboring chains (for a detailed packing diagram, see Figure S2 in the Supporting Information). Each of the two nitrogen atoms of 2,2′-bipy$^{\bullet-}$, N1 and N2, binds to two potassium cations, K1 and K1A (generated by symmetry). Bond distances between K1 and N1 and N2 are 2.820(2) and 2.841(2) Å, respectively, and can be largely considered as σ interactions with the nitrogen lone pairs. The distances between K1A and N1 and N2 are both 2.960(2) Å and arise from interactions with the radical π system, judging by the geometric disposition of the cation and anion. There are also two relatively short contacts between K1A and the C5 and C6 atoms of the 2,2-bipyridyl radical, with

(25) Stoll, S.; Schweiger, A. *J. Magn. Reson.* **2006**, *178*, 42.
(26) Constable, E. C. Homoleptic Complexes of 2,2′-Bipyridine. In *Advances in Inorganic Chemistry*; Sykes, A. G., Ed.; Academic Press: San Diego, 1989; Vol. *34*, p 1.
(27) (a) McWhinnie, W. R.; Miller, J. D. *Adv. Inorg. Chem. Radiochem.* **1969**, *12*, 135. (b) Herzog, S.; Taube, R. *Z. Chem.* **1962**, *2*, 208.

Table 1. Selected X-ray Data Collection and Refinement Parameters for **1a**, **1b**, and **2**

compound	K(2,2′-bipy)(en)	K_4(2,2′-bipy)$_4$(en)$_4$	Rb(2,2′-bipy)$_{0.5}$(en)
fw	255.39	1021.55	223.67
space group, Z	$P2(1)/c$, 4	$P2(1)/c$, 4	$P\bar{1}$, 2
a (Å)	9.7584(2)	14.7111(1)	6.2046(3)
b (Å)	15.2777(4)	18.6597(2)	7.6321(3)
c (Å)	8.9523(2)	21.5292(3)	9.5740(5)
α (deg)	90.000	90.000	96.819(2)
β (deg)	104.000(1)	118.910(1)	99.593(2)
γ (deg)	90.000	90.000	104.053(2)
V (Å^3)	1295.02(5)	5173.38(10)	427.60(4)
ρ_{calc} (g cm^{-3})	1.310	1.312	1.737
radiation, λ (Å)		Mo Kα, 0.710 73	
temp (K)	200	150	150
μ (mm^{-1})	0.394	0.395	5.728
reflns collected	4435	22852	3363
indep reflns	2264	11654	1932
R(int)	0.0164	0.0320	0.0420
R1/wR2,[a] $I \geq 2\sigma(I)$ (%)	4.24/11.38	4.00/9.25	3.98/10.22
R1/wR2,[a] all data (%)	5.15/12.12	7.54/10.43	4.16/10.41

[a] $R1 = [\sum||F_o| - |F_c||]/\sum|F_o|$; $wR2 = \{[\sum w[(F_o)^2 - (F_c)^2]^2]/[\sum w(F_o^2)^2]\}^{1/2}$; $w = [\sigma^2(F_o)^2 + (AP)^2 + BP]^{-1}$, where $P = [(F_o)^2 + 2(F_c)^2]/3$ and the A and B values are 0.0708 and 0.5042 for **1a**, 0.0424 and 1.6659 for **1b**, and 0.0603 and 0.3478 for **2**.

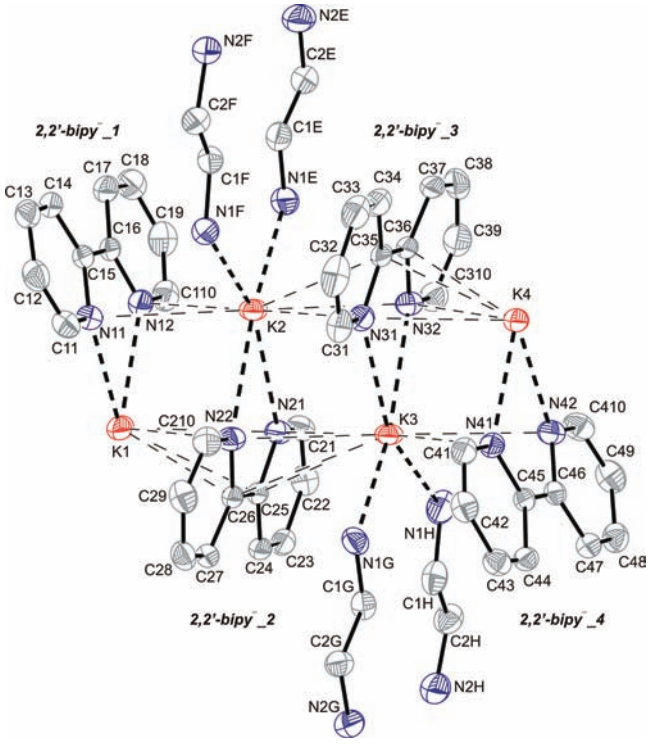

Figure 2. Thermal ellipsoid representation of the atoms in the asymmetric unit of **1b**. Anisotropic displacement ellipsoids pictured at the 50% probability level. Hydrogen atoms have been omitted for clarity.

distances of 3.337(2) and 3.314(2) Å, respectively. Each dimer is linked to its nearest neighbor by bridging en molecules, which bind to atom K1 via N1E, 2.851(3) Å, and to K1A from the nearest dimeric unit via N2E, 2.892(2) Å. In this crystal structure, as in all of the others that we will discuss in this manuscript, en molecules play a significant role in network bonding because of their ability to act as polydentate Lewis bases. The flexibility of the ethylene backbone allows the molecules to act as both linkers and chelates, making them versatile "building blocks" in the isolation of crystalline samples. This structural plasticity has also been found to give rise to numerous polymorphs for compounds of a given chemical composition (e.g., **1a** and **1b**). The influence of ether-based Lewis acids over the solid-state structures of alkali-metal complexes has been well documented in the chemical literature,[28] yet the role played by solvents such as en in alkali-metal networks is less well studied because there are fewer known structures.[18,29] Crystals for **1a** were found to crack at temperatures below 200 K, presumably because of the onset of a phase transition. Similar reversible phase transitions have been previously reported for related compounds such as Na_2(4,4′-bipy)-(en)$_2$.[18] The bond distances within the radical anion are best discussed in the context of other neutral 2,2'-bipy species and the dianionic species present in **2**, which we will address in detail below.

The structure of the second polymorph isolated from the reaction of 1 mol equiv of potassium with 2,2'-bipy, **1b**, appears slightly more complex at first glance, but upon inspection, it becomes apparent that there are clear similarities between **1a** and **1b**. The asymmetric unit of **1b** contains four crystallographically unique potassium cations, four 2,2′-bipyridyl radical anions, and four terminally bonding en molecules (Figure 2). These fragments give rise to tetrameric building blocks that link together via bridging en molecules to give rise to a two-dimensional sheetlike structure. The two-dimensional sheets run along the crystallographic *ab* plane and stack along the *c* axis of the unit cell, giving rise to an extended structure that exhibits no interactions between the two-dimensional networks (a detailed packing diagram is provided in the Supporting Information). The tetrameric units are largely held together via interactions between potassium cations and the π manifolds of neighboring

(28) For example, see: (a) McGarrity, J. F.; Ogle, C. A. *J. Am. Chem. Soc.* **1985**, *107*, 1805. (b) Bates, R. B.; Ogle, C. A. *Carbanion Chemistry*; Springer Verlag: Berlin, 1983. (c) Jackman, L. M.; Lange, B. C. *Tetrahedron* **1977**, *33*, 2737. (d) Wardell, J. L. In *Comprehensive Organometallic Chemistry*; Wilkinson, G., Stone, F. G. A., Abel, E. W., Eds.; Pergamon Press: Oxford, U. K., 1982; Vol. *1*, p 43.

(29) (a) Buchholz, S.; Harms, K.; Marsch, M.; Massa, W.; Boche, G. *Angew. Chem., Int. Ed.* **1989**, *28*, 72. (b) Giese, H. H.; Habereder, T.; Knizek, J.; Nöth, H.; Warchhold, M. *Eur. J. Inorg. Chem.* **2001**, 1195. (c) Wang, C.; Haushalter, R. C. *Inorg. Chem.* **1997**, *36*, 3806. (d) Jones, C. D. W.; DiSalvo, F. J.; Haushalter, R. C. *Inorg. Chem.* **1998**, *37*, 821. (e) Rabe, G. W.; Heise, H.; Yap, G. P. A.; Liable-Sands, L. M.; Guzei, I. A.; Rheingold, A. L. *Inorg. Chem.* **1998**, *37*, 4235.

bipyridyl radicals. In these tetrameric units, each potassium cation binds to a single chelating 2,2′-bipyridyl radical via two σ interactions with the nitrogen atom lone pairs. Thus, K1 binds to the two nitrogen atoms of a 2,2′-bipyridyl moiety, N11 and N12. Similarly, K2 binds to a different 2,2′-bipy$^{\bullet-}$ via N21 and N22. Finally, K3 and K4 also interact with two crystallographically unrelated bipyridyl radicals via N31 and N32 and via N41 and N42, respectively. The lengths of these σ interactions vary between 2.765(2) and 2.951(2) Å, with a mean value of 2.829 Å. In addition to these σ interactions, there are also a substantial number of close interactions between potassium cations and the π systems of neighboring 2,2′-bipy$^{\bullet-}$ moieties. These interactions have been highlighted as thin dashed lines in Figure 2. The distances between the potassium cations and the nitrogen atoms with which they make "side-on" contact vary between 3.090(2) and 3.360(2) Å, with a mean value of 3.197 Å. A certain degree of bonding may also be inferred by the interactions between the potassium cations and the carbon atom backbones of neighboring 2,2′-bipyridyl radicals. These distances were found to lie between 3.015(2) and 3.450(2) Å, with a mean value of 3.236 Å. These interactions have also been highlighted as thin dashed lines in Figure 2 (all distances between potassium cations and carbon atoms greater than 3.5 Å were ignored). These tetrameric units give rise to two-dimensional networks via terminally binding en molecules, which link them together. Each potassium cation binds to two en molecules, which bind terminally as monodentate linkers. The remaining nitrogen atom of each en molecule terminally binds to an adjacent tetrameric cluster. Thus, the potassium cation K1 from one tetramer and the potassium cation K2 from an adjacent tetramer are linked via two en molecules. Similarly, K3 and K4 from adjacent tetramers are also linked via bridging en molecules. The bond distances for these interactions vary between 2.876(2) and 2.951(2) Å. A closer inspection of the extended structure of **1b** reveals that the structure may also be interpreted as zig-zag one-dimensional chains (similar to those observed in **1a**) in which there are clear interactions between adjacent chains (see Figure S3 in the Supporting Information).

During the course of these studies, we also managed to isolate the 2,2′-bipyridyl dianion as a rubidium salt in **2** (Figure 3). This dianionic species was first crystallographically characterized by Bock, Lehn, and co-workers in three different sodium-containing species, all of which were obtained by the direct reduction of 2,2′-bipy with an alkali metal.[7] Species **2** exhibits a single crystallographically unique rubidium cation in the asymmetric unit, Rb1, which is accompanied by half of a 2,2′-bipy moiety and an en molecule. These building blocks give rise to a two-dimensional layered structure that has sheets running along the crystallographic *ab* plane. Such two-dimensional networks stack along the crystallographic *c* axis with no interactions between adjacent layers (for a detailed packing diagram, see Figure S5 in the Supporting Information). In species **2**, the 2,2′-bipyridyl dianion, 2,2′-bipy^{2-}, adopts a trans conformation, with the nitrogen atoms pointing in opposite directions, arguably because of the partial localization of the negative charge of the more electronegative nitrogen atoms. Interestingly, the three structures reported by Bock and Lehn all exhibit

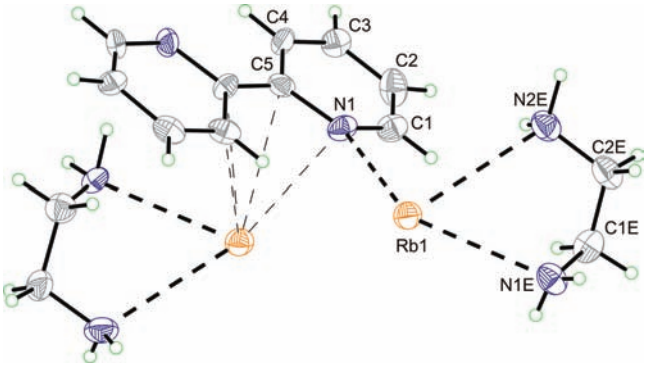

Figure 3. Thermal ellipsoid representation of the repeating structural motif in **2**. Anisotropic thermal displacement ellipsoids pictured at 50% occupancy. Only the crystallographically unique non-hydrogen atoms are labeled.

cis conformations, implying that the thermodynamic benefit of having the nitrogen atoms opposite to one another may not be that substantial and that crystal packing effects may play a much greater role. The trans conformation in **2** allows each dianionic fragment to bridge rubidium metal centers via σ interactions. Bridging en molecules connect these units, giving rise to one-dimensional chains. Each en molecule bridges two rubidium metal centers via both nitrogen atoms as a chelating bridge. As a result, N1E and N2E bind to one rubidium cation with distances of 3.081(3) and 3.164(3) Å, respectively, and to a neighboring rubidium cation with distances of 3.180(3) and 3.110(3) Å, respectively. Further interactions between the π manifolds of bipyridyl dianions and adjacent rubidium metal centers ultimately give rise to the two-dimensional networks observed throughout the structure. These interactions have been highlighted in Figure 3, and a more detailed packing diagram is provided in the Supporting Information. The two different interactions between N1 and Rb1 exhibit comparable bonding distances of 2.946(3) and 2.976(3) Å, respectively. Further evidence of the interactions of the alkali-metal cations with the dianion π system can be observed between Rb1 and carbon atoms C4, C5, and C5A (generated by symmetry), which exhibit "bonding" distances of 3.225(3), 3.236(3), and 3.131(3) Å, respectively.

Electronic Structure and Bond Metric Parameters. Close inspection of the crystallographic structures recorded for **1a**, **1b**, and **2** shows a clear correlation between the bond metric parameters of the 2,2′-bipyridyl moieties and the charge associated with each species. As would be expected upon reduction of 2,2′-bipy, its lowest unoccupied molecular orbital (LUMO) would become the singly occupied molecular orbital (SOMO) of the 2,2′-bipyridyl radical, and, in the absence of a degenerate orbital, the highest occupied molecular orbital (HOMO) of the dianion. This orbital corresponds to a nondegenerate π*-antibonding orbital, pictured in Figure 4b. Upon occupation of this orbital by the electron(s) donated by an alkali-metal reagent, one would expect the in-phase π interactions to have a greater bonding character, which would be manifested in shorter bond distances, and the out-of-phase interactions to become more antibonding, manifested in longer bond distances. Consequently, if we

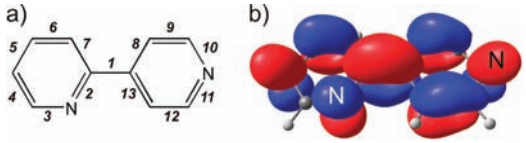

Figure 4. (a) Numbering scheme employed to discuss metric bond data for all of the 2,2′-bipyridine-derived species. (b) 2,2′-bipy LUMO highlighting the alternating bonding and antibonding interactions of the π system.

Table 2. Bond Lengths [Å] for 2,2′-bipy and the 2,2′-bipy$^{\bullet-}$ and 2,2′-bipy^{2-} Moieties in Species **1a**, **1b**, and **2**[a]

		2,2′-bipy$^{\bullet-}$		2,2′-bipy^{2-}
bond[b]	2,2′-bipy[c]	**1a**	**1b**[d]	**2**
1	1.490(3) [1.494]	1.431(3)	1.429(av) [1.436]	1.399(6) [1.400]
2	1.346(2) [1.357]	1.388(3) 1.391(3)	1.388(av) [1.403]	1.436(4) [1.442]
3	1.341(2) [1.350]	1.338(3) 1.336(3)	1.337(av) [1.341]	1.343(4) [1.339]
4	1.384(2) [1.397]	1.374(3) 1.372(3)	1.382(av) [1.405]	1.381(5) [1.412]
5	1.383(3) [1.397]	1.403(4) 1.405(3)	1.404(av) [1.419]	1.429(5) [1.440]
6	1.385(2) [1.395]	1.366(3) 1.363(3)	1.364(av) [1.382]	1.358(5) [1.376]
7	1.394(2) [1.407]	1.428(3) 1.427(3)	1.428(av) [1.438]	1.452(4) [1.453]

[a] Data in brackets correspond to the bond lengths [Å] obtained from the optimized geometries using the computational methods described in the manuscript. [b] Bond numbering scheme, as indicated in Figure 5a. [c] Bond metric data taken from ref 16a. [d] Average values given for the four crystallographically unique 2,2′-bipyridyl radicals present in the asymmetric unit of **1b**.

employ a bond numbering scheme such as the one pictured in Figure 4a, upon successive reduction steps, we would expect bonds 1 and 6 to shorten and bonds 2, 5, and 7 to elongate. This is indeed the case, and we clearly observe substantial changes to these particular bipyridyl C−C and C−N bond distances as a direct result of the chemical reduction of the neutral parent species (a complete list of pyridyl ring bond distances for compounds **1a**, **1b**, and **2** is given in Table 2). Furthermore, it is also apparent that, upon a second reductive step, reduction of the 2,2′-bipyridyl radical to the 2,2′-bipyridyl dianion, these effects are even more pronounced, indicating the additional occupation of this orbital by a second electron. This effect is most prominent for the interpyridyl ring distance labeled as bond 1 in Figure 4a. This bond shrinks from a single bond in the neutral compound, with a distance of 1.490(3) Å, to a much shorter partially π-bonding interaction for species **1a** and **1b**, which exhibit distances of 1.431(3) and 1.429(2) Å, respectively. Finally, following reduction to the dianion, this bond effectively adopts a double-bond character, exhibiting a bond distance of 1.399(6) Å, an effective variation of 0.091 Å, or a 6% change compared to the neutral parent compound. The value observed for the interpyridyl ring bond distance of the dianionic species **2** is very much in line with those reported by Bock and Lehn for the three 2,2′-bipyridyl-dianion-containing species that they isolated, which exhibited values of 1.375, 1.382(av), and 1.376 Å.[7] It is also very similar to the value of 1.407(av) Å reported for $[\{Yb(\mu^2\text{-}N_2C_{10}H_8)(THF)_2\}_3]$.[8] Similarly, the interpyridyl ring bond distances of 1.431(3) and 1.429(2) Å observed for the radical anion complexes **1a** and **1b** are also very much in line with the values of 1.429(4), 1.436(9), 1.425(av), and 1.417(3) Å observed for $(Cp^*)_2Sm(2,2'\text{-bipy})$,[14] $(Cp^*)_2Yb(2,2'\text{-bipy})$,[15a] $Mo(O^iPr)_2(2,2'\text{-bipy})_2$,[16a] and $(\eta^6\text{-Tol})Fe(2,2'\text{-bipy})$ (Tol = toluene),[16b] respectively, all of which can formally be discussed as complexes of the bipyridyl radical anion. These arguments can be extended to the rest of the C−C and C−N bond distances of the 2,2′-bipyridyl moieties of compounds **1a**, **1b**, and **2** and can be observed in the bond metric data provided in Table 2.

The bond metric values observed are consistent with those calculated for the optimized geometries of the neutral, radical and dianionic species using standard computational methods. DFT studies on neutral 2,2′-bipy reveal an accessible nondegenerate LUMO such as the one pictured in Figure 4b, which is comprised of π-orbital contributions from the majority of the heterocyclic atoms. Additional calculations on 2,2′-bipy$^{\bullet-}$ and 2,2′-bipy^{2-} reveal an orbital identical with SOMO and HOMO, respectively. Furthermore, the bond distances calculated for the optimized geometries for all three species are also consistent with the trends observed in the crystallographically characterized complexes. These data are also provided in Table 2.

An additional measure of the reduced character of a given bipyridyl moiety may also be sought in the torsion angle between pyridyl rings. Upon reduction, the interpyridyl ring bond, bond 1, becomes more strongly π bonding, and as a result, the two pyridyl rings should adopt a coplanar geometry. However, this phenomenon is not strongly manifested in the case of the 2,2′-bipyridyl isomer for several reasons, the most important of which is the chelating character of neutral 2,2′-bipy. In most complexes, this species acts as a chelating ligand that requires a fair degree of pyridyl ring coplanarity to achieve optimum bonding. As a result, the torsion angle values observed by single-crystal X-ray diffraction for species containing the neutral 2,2′-bipy ligand are relatively small. A search of the CCDC revealed a mean torsion angle of 4.4°.[30] A comparison of this value with those of 5.6°, 1.8°, and 0° observed for **1a**, **1b**, and **2**, respectively, reveals no significant variations, and as a result, this metric cannot be used diagnostically.

Spectroscopic Characterization. EPR measurements of solutions of 2,2′-bipy in the presence of alkali metals such as lithium or sodium provided the first spectroscopic evidence for the existence of the 2,2′ radical anion.[12] The ability of this highly sensitive technique to register the presence of trace amounts of a paramagnetic species provided a useful probe that allowed for the early characterization of this and many other organic radicals in solution. Naturally, our first spectroscopic measurements on sample **1** were solution and solid-state EPR measurements in order to confirm the presence of 2,2′-bipy$^{\bullet-}$. Both measurements unequivocally prove the existence of the radical anion in the sample and exhibit g values very close to that of the free electron (g = 2.002 319). Solution EPR measurements registered a g value of 2.0035, with a characteristic hyperfine splitting pattern arising from the

(30) Average of 4192 hits from CSD, version 5.30 (Nov **2008**).

coupling of the unpaired electron with the nuclear spins of ^{14}N ($I = 1$) and ^{1}H ($I = {}^{1}/_{2}$). The isotropic Fermi contact coupling constants, as calculated by DFT, were found to be in very close agreement with those obtained following a least-squares fitting of the experimentally determined spectrum of the radical anion. DFT calculations predict a coupling constant of 8.74 MHz for the coupling of the spin magnetic moment with the ^{14}N nuclear spins and values of −4.65, −0.98, 14.54, and 2.42 MHz for coupling to the proton nuclei in positions 3−6, respectively. The coupling constant values obtained following a least-squares fit of the experimentally determined spectrum were 9.03 MHz for coupling to ^{14}N and −4.32, −1.77, −15.9, and 0.32 MHz for ^{1}H couplings (a plot of experimentally determined and calculated EPR spectra is provided in Figure S6 in the Supporting Information). These values are in good agreement with similar literature values reported for the 2,2′-bipyridyl radical.[12]

Similarly, EPR measurements on a solid sample of **1** also showed an EPR resonance with a similar *g* value of 2.0033 (see Figure S8 in the Supporting Information). This resonance exhibits a certain degree of anisotropy, which we believe may arise from one of two possible scenarios. The first possibility is that the anisotropy of the resonance observed for **1** is a consequence of having a mixture of two solid products, **1a** and **1b**. These species could conceivably exhibit two slightly different resonances that overlap, giving rise to an asymmetric signal. The second possibility is that the resonance anisotropy is a result of a single solid product (we believe species **1b** is the predominant crystalline product) that has different parallel and perpendicular contributions to the overall *g* value. This would be consistent with the highly ordered crystal structure exhibited by **1b**, which clearly shows that all bipyridyl radicals are stacked perpendicularly to the *ab* plane. Regardless of the origin, these measurements provide unequivocal proof of the existence of the radical anion both in solution and in the solid state. Interestingly, EPR measurements on a solid sample of the dianion (**2**), which we would expect to be diamagnetic, also show evidence of a very weak resonance in the EPR spectrum. This resonance has a *g* value of 2.0033 and is extremely weak by comparison to sample **1**. We believe that this resonance may arise from trace amounts of the radical anion in the lattice of **2**, giving rise to a structure of nominal composition $Rb_{2-x}(2,2'\text{-bipy}^{2-})_{1-x}(2,2'\text{-bipy}^{\bullet-})_x(en)_2$. This is unsurprising considering the highly sensitive nature of EPR as a characterization technique, which is capable of registering the presence of paramagnetic centers at concentrations as low as 10^{-9} M.[31]

In recent years, the amount of spectroscopic data available for the 2,2′-bipyridyl radical has proven a useful resource for researchers who have questioned ligand oxidation states in low-valent coordination compounds of 2,2′-bipy. Particular attention has been paid to the work by Nakamoto and co-workers, whose IR spectroscopy studies have proven to be an extremely useful diagnostic tool.[9] In their frequently cited paper, they argue that two particular regions of the IR spectrum can be employed to ascertain whether a coordination complex formally corresponds to a complex of neutral 2,2′-bipy or of the radical anion, 2,2′-bipy$^{\bullet-}$. The first of these regions is between 900 and 1000 cm^{-1}, where there are no absorptions observed for neutral 2,2′-bipy. Interestingly, reduced species such as Li(bipy)·*n*THF show a peak corresponding to a ring deformation mode in this region (944 cm^{-1} for Li(bipy)·*n*THF). An IR sample of compound **1** revealed an absorption peak at 939 cm^{-1}, which is consistent with this analysis. The second diagnostic region is the C=C and C=N stretching region between 1475 and 1625 cm^{-1}. According to Nakamoto, a complex of neutral 2,2′-bipy should exhibit a relatively strong absorption band between 1600 and 1610 cm^{-1} while a complex of the radical anion would exhibit several medium-to-strong intensity bands in the 1490−1575 cm^{-1} region. This is also observed for compound **1**, which exhibits two bands at 1495 and 1561 cm^{-1}. Two coinciding peaks were also observed in the Raman spectrum at 1495 and 1560 cm^{-1}, which are also consistent with the values of 1486 and 1554 cm^{-1} reported in the literature for the resonance Raman spectrum of Li(bipy).[10,16a] The IR and Raman spectra observed for compound **1** are complicated because of the presence of absorption peaks corresponding to the vibrational modes of the en molecules present in the crystal lattice; however, a comparison with the literature-reported data shows many common features.

In contrast to the 2,2′-bipyridyl radical, there is a dearth of spectroscopic data available in the chemical literature for the 2,2′-bipyridyl dianion, 2,2′-bipy^{2-}. During the course of our studies, we collected the IR and Raman spectra for sample **2**, which contains the anti or trans isomer of the 2,2′-bipyridyl dianion (a comprehensive list of this data is presented in the Experimental Section). The trans conformation of the 2,2′-bipyridyl dianion belongs to the C_{2h} point group, which contains a center of inversion. As a result, the mutual-exclusion rule applies and there should be no coincidental peaks observed in the corresponding IR and Raman spectra. This is observed in the spectra of **2** because both the IR and Raman spectra are notably different. A very small number of peaks that appear in both spectra presumably arise from the en solvent molecules present in the crystal structure. The IR spectrum reveals several diagnostic peaks for the dianionic species. There are two strong peaks at 1560 and 1590 cm^{-1} arising from C=C and/or C=N stretches. These are much more intense and have been shifted to higher wavenumbers than those observed for the radical anion. There are also several peaks between 800 and 900 cm^{-1}, which are absent from the IR spectra of the 2,2′-bipyridyl radical and neutral 2,2′-bipy, that may be used diagnostically to recognize the presence of the dianion. These occur at 801, 830, and 867 cm^{-1} and are unique to the IR spectrum of the dianionic species. The Raman spectrum of **2** reveals three intense peaks at 1434, 1493, and 1578 cm^{-1} in addition to several other very strong peaks at 433, 709, 957, 1083, and 1233 cm^{-1}. Of these, the resonance at 957 cm^{-1} seems diagnostic of the dianion, as has been previously reported for Li_2(bipy).[10c]

3.2. 2,4′-Bipyridyl Radical Anion and Dianion. Synthesis and Crystallographic Characterization. Employing a method analogous to that used for the synthesis of the

(31) Weil, J. A.; Bolton, J. R. *Electron Paramagnetic Resonance: Elementary Theory and Practical Applications*, 2nd ed.; Wiley: Hoboken, NJ, 2007.

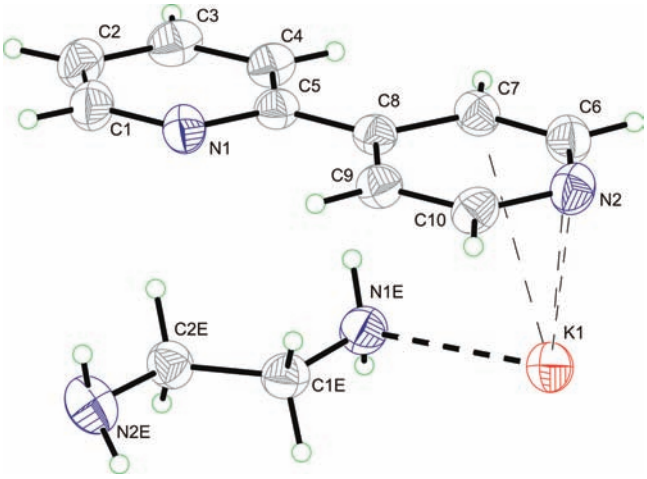

Figure 5. Thermal ellipsoid representation of the atoms in the asymmetric unit of **3**. Anisotropic displacement ellipsoids pictured at the 50% probability level.

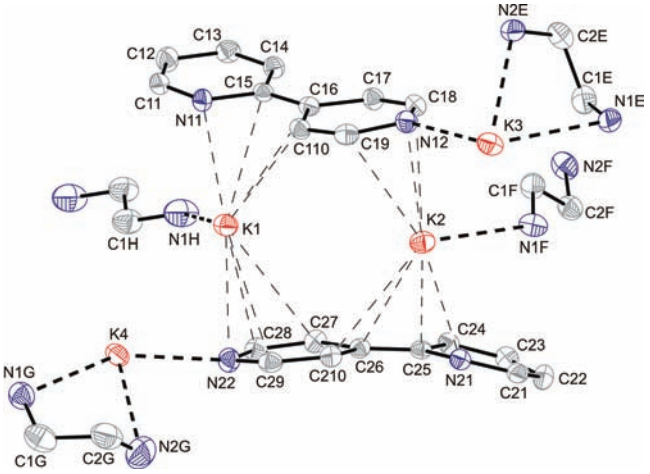

Figure 6. Thermal ellipsoid representation of the repeating structural motif in **4**. Anisotropic thermal displacement ellipsoids pictured at 50% probability level. Hydrogen atoms have been omitted for clarity. Only the crystallographically unique non-hydrogen atoms are labeled.

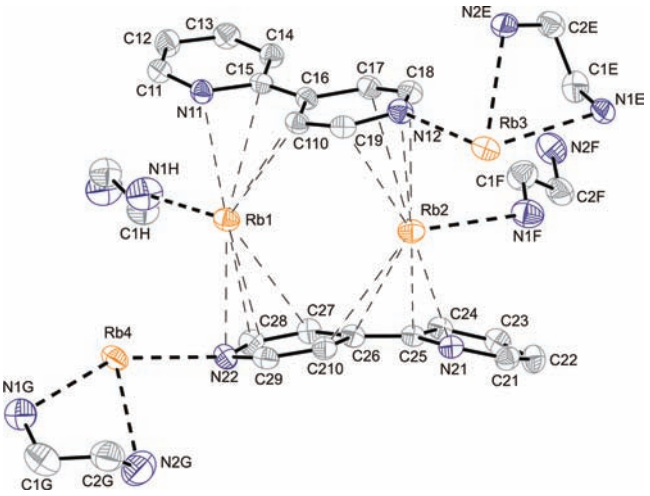

Figure 7. Thermal ellipsoid representation of the repeating structural motif in **5**. Anisotropic thermal displacement ellipsoids pictured at 50% probability level. Hydrogen atoms have been omitted for clarity. Only the crystallographically unique non-hydrogen atoms are labeled.

2,2′-bipyridyl radical anion and dianion, we were also able to isolate the corresponding 2,4′-bipyridyl congeners. The reaction of 1 equiv of potassium metal with 2,4′-bipy in en was found to yield the 2,4′-bipyridyl-radical-containing species **3** (Figure 5). This species can be obtained in moderate crystalline yields by layering crude reaction mixtures with toluene or ether. The bulk composition of the crystalline sample was confirmed by powder X-ray diffraction and elemental analysis, revealing a clean conversion to a single crystallographic phase (see Figure S13 in the Supporting Information for predicted and experimental powder X-ray diffraction patterns).

Similar reactions with greater excess of an alkali-metal reagent (2 mol equiv or above) were found to yield the 2,4′-bipyridyl dianion. This species was isolated as two isostructural salts of potassium and rubidium in A_4(2,4′-bipy)$_2$(en)$_{3.5}$ [A = K (**4**), Rb (**5**)]. Both species exhibit largely the same structural properties, as evidenced by a comparison of their asymmetric units, pictured in Figures 6 and 7 for potassium and rubidium, respectively. Crystallographic data and collection parameters for these structures are presented in Table 3. The compositional purity of the samples was determined by elemental analysis for both samples, and a powder X-ray diffraction pattern was also collected for sample **5** in order to rule out the presence of other possible, compositionally identical, crystalline phases (see Figure S14 in the Supporting Information).

The crystal structure exhibited by **3** displays a single 2,4′-bipyridyl radical anion in the asymmetric unit accompanied by a charge-balancing cation, K1, and an en solvent molecule, as pictured in Figure 5. The sample crystallizes in the orthorhombic space group *P*2(1)2(1)2(1) and exhibits an extended three-dimensional structure with interactions between the alkali-metal cations and both the nitrogen atom lone pairs and the π manifold of the bipyridyl radicals. Interestingly, the three-dimensional nature of this structure relies exclusively on bonding between the nitrogen in position 4′ of the bipyridyl radical, N2, and the potassium metal cations, with en molecules also acting as bridges between metal centers. No active role in network bonding is played by the nitrogen atom in position 2 (N1). In the crystal structure, each N2 atom acts as a bridge between two different, symmetry-related, potassium cations via what appears to be a largely σ-bonding interaction between the nitrogen atom lone pair and one potassium metal cation and an interaction to another cation via the π system. The representation of the asymmetric unit of **3**, shown in Figure 5, clearly shows the π-manifold interaction between K1 and N2 as a thin dashed line. The distances for these two different interactions are 2.800(2) and 3.249(2) Å for the σ interaction and the "side-on" contact, respectively. The nitrogen atoms from each en molecule, N1E and N2E, also act as bridges between potassium cations, with each one of the two nitrogen atoms bonding terminally to different metal cations. As a result, N1E binds to K1 with a bond distance of 2.798(2) Å and N2E binds to a different, crystallographically related cation, with a distance of 2.882(2) Å. These interactions ultimately give rise to a three-dimensional distorted diamondoid network, where each potassium metal cation is

Table 3. Selected X-ray Data Collection and Refinement Parameters for **3**−**5**

compound	K(2,4′-bipy)(en)	K_4(2,4′-bipy)$_2$(en)$_{3.5}$	Rb_4(2,4′-bipy)$_2$(en)$_{3.5}$
fw	255.39	679.13	864.61
space group, Z	$P2(1)2(1)2(1)$, 4	$P2(1)/c$, 4	$P2(1)/c$, 4
a (Å)	6.9699(2)	13.6287(1)	14.0310(2)
b (Å)	9.3455(2)	20.0334(3)	20.3177(3)
c (Å)	19.0541(5)	13.7395(2)	13.5537(2)
α (deg)	90.000	90.000	90.000
β (deg)	90.000	118.718(1)	117.447(1)
γ (deg)	90.000	90.000	90.000
V (Å^3)	1241.13(6)	3289.86(7)	3428.93(9)
ρ_{calc} (g cm^{-3})	1.367	1.371	1.675
radiation, λ (Å)		Mo Kα, 0.710 73	
temp (K)	150	150	150
μ (mm^{-1})	0.411	0.578	5.711
reflns collected	2811	14 414	15 302
indep reflns	2811	7497	7795
R(int)	0.00	0.0303	0.0456
R1/wR2,[a] $I \geq 2\sigma(I)$ (%)	4.00/9.70	4.02/9.55	3.92/9.30
R1/wR2,[a] all data (%)	4.70/10.25	6.52/10.66	5.65/10.08

[a] $R1 = [\sum||F_o| - |F_c||]/\sum|F_o|$; $wR2 = \{[\sum w[(F_o)^2 - (F_c)^2]^2]/[\sum w(F_o^2)^2]\}^{1/2}$; $w = [\sigma^2(F_o)^2 + (AP)^2 + BP]^{-1}$, where $P = [(F_o)^2 + 2(F_c)^2]/3$ and the A and B values are 0.0511 and 0.2496 for **3**, 0.0493 and 1.3650 for **4**, and 0.0459 and 2.9749 for **5**.

pseudotetrahedrally coordinated by four nitrogen atoms [N1E, N2E, N2 (via lone pair), and N2 (via π-manifold)] from substituents that act as bridges to four different, but crystallographically related, potassium cations (for a more detailed bonding diagram, see the Supporting Information). Because of the lack of strongly directional covalent interactions, the flexible character of the bridging en substituents and the different lengths of bridging en and bipyridyl moieties, the three-dimensional structure is highly distorted from an ideal diamondoid network. This can be observed in the bond angles of the nitrogen substituents around a given potassium metal cation, which vary between 79.58(6)° and 165.90(6)° for N2−K1−N2E and N1E−K1−N2, respectively. The average value for all six tetrahedral angles is 108.00°. In addition to the bonds discussed, there is also some evidence for a short metal−carbon interaction arising between K1 and the carbon atoms labeled as C6 and C7 from one 2,4′-bipyridyl radical moiety (K−C bond distances of 3.078(2) and 3.348(2) Å, respectively) and between K1 and C10 from an adjacent bipyridyl moiety [3.381(2) Å]. Bond distances within the 2,4′-bipyridyl radical moiety are best discussed in relation to those of the neutral parent compound and the dianionic species isolated in compounds **4** and **5** and will be discussed in depth below.

Because of the isostructural nature of compounds **4** (Figure 6) and **5** (Figure 7), their single-crystal X-ray structures can be addressed simultaneously, and we will limit ourselves to discussing the bonding interactions present within **4**. In addition to two 2,4′-bipyridyl dianions, the asymmetric unit of **4** also contains four unrelated potassium cations and three and a half crystallographically unique en molecules. This asymmetric unit gives rise to an extended three-dimensional network that is held together by interactions between potassium metal cations and dianionic 2,4′-bipyridyl moieties. As with many of the crystal structures discussed previously, the en molecules present in the lattice play an important role in network bonding, acting as bridges between metal centers.

The three-dimensional crystal structure of **4** appears quite complex upon first examination; however, it can be simplified by describing it as comprised of two-dimensional sheets that run along the crystallographic *ac* plane of the unit cell. These sheets ultimately give rise to an extended three-dimensional network because of the role played by two different bridging en molecules (labeled as F and H in Figure 6) that terminally bind to potassium metal cations from adjacent sheets, building up the structure along the crystallographic *b* axis. (N1F binds to K2, while N2F binds to K3; N1H bonds to two crystallographically distinct K1 cations.) Each two-dimensional sheet involves extensive interactions between the four potassium cations and the lone pairs and π systems of the two crystallographically unique 2,4′-bipyridyl moieties pictured in Figure 6. In addition, there is also an active role played by the en molecules labeled as E and G in Figure 6. These molecules act as chelating bridges between potassium cations, which along with the interactions between potassium metal cations and π systems of the bipyridyl dianions help extend the crystal structure along one dimension. As a result, N1E and N2E both act as linkers between K3 and K4, with distances ranging between 2.941(2) and 2.986(2) Å. Similarly, N1G also bridges K3 and K4, with bond distances ranging between 2.864(2) and 3.068(2) Å. (The bond distance between N2G and K3 is too long to consider it a bridging interaction.) Of the four crystallographically unique potassium cations, K1 and K2 exhibit a large degree of "side-on" bonding interactions to the 2,4′-bipyridyl dianions pictured, as shown in Figure 6. K1 interacts with N11, C15, C16, and C110 of one bipyridyl dianion with bond distances that range between 2.832(2) and 3.259(2) Å and with N22, C27, C28, and C29 from a different bipyridyl moiety, with bond distances ranging between 2.998(2) and 3.478(2) Å (all K−C and K−N distances greater than 3.5 Å have been ignored). A σ interaction with a bond distance of 2.834(2) Å between N21 from an adjacent 2,4′-bipyridyl dianion and K1 is also present, helping to extend the structure in a second dimension. Similarly, K2 also sits between two bipyridyl dianions and exhibits interactions to the π manifold through N12, C18, and C19 with bond distances of 2.861(2), 3.067(2), and 3.157(2) Å, respectively, and through N21, C25, C26, and C210 with distances ranging between 2.827(2) and

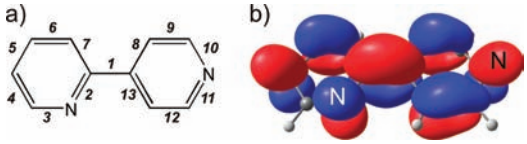

Figure 8. (a) Numbering scheme employed to discuss metric bond data for all of the 2,4′-bipy-derived species. (b) 2,4′-bipy LUMO highlighting the alternating bonding and antibonding interactions of the π system.

3.268(2) Å. A σ bond between K2 and N11 from an adjacent symmetry-generated bipyridyl dianion is also present with a distance of 2.860(2) Å. Analogously to the σ interaction between K1 and N21, this bond also serves to generate the two-dimensional sheets. Cations K3 and K4 are involved in clear σ interactions with the nitrogen atoms in the 4′ positions of the dianionic moieties. Thus, K3 binds to N12 and K4 binds to N22 with bond distances of 2.925(2) and 2.816(2) Å, respectively. Additional interactions between K3 and the π manifold of a 2,4′-bipyridyl dianion are also present, with interactions arising between K3 and N11, C14, C15, and C16 ranging between 2.945(2) and 3.497(2) Å. Similarly, there are also analogous interactions arising between K4 and N21, C21, C25, C26, and C210, with distances that vary between 2.942(2) and 3.409(2) Å. To summarize, K1 and K2 form σ bonds with the nitrogen atoms in the 2 position of the 2,4′-bipyridyl moieties and, conversely, K3 and K4 form σ bonds with the nitrogen atoms in the 4′ positions. All four metal cations partake in extensive bonding to the π manifolds of the dianionic units, which ultimately gives rise to a two-dimensional sheetlike structure. These sheets are held together by terminally bridging en molecules that extend the structure in a third dimension (a diagrammatic representation of the bonding within this structure is provided in Figure S16 of the Supporting Information).

Electronic Structure and Bond Metric Parameters. As we discussed previously regarding the chemically reduced forms of 2,2′-bipy, a clear correlation can be drawn between the bond metric data obtained for the radical (compound **3**) and dianionic (compounds **4** and **5**) forms of 2,4′-bipy and their frontier molecular orbitals. A representation of the LUMO for neutral 2,4′-bipy is pictured in Figure 8b. DFT calculations similar to those carried out on 2,2′-bipy indicate that this is the same orbital that acts as the SOMO for the 2,4′-bipyridyl radical and the 2,4′-bipyridyl dianion HOMO. As a result, the chemical reduction of neutral 2,4′-bipy results in large changes to the bonding or antibonding character of the C−C and C−N chemical bonds of the 2,4′-bipyridyl moieties (a numbering scheme for the different bonds of the bipyridyl moieties is provided in Figure 8a).[32] From inspection of this important frontier molecular orbital, it is apparent that upon reduction one would expect bonds 1, 6, 9, and 12 of the 2,4′-bipyridyl units to shorten upon reduction. Similarly, bonds 2, 5, 7, 8, 10, 11, and 13 should elongate. Inspection of Table 4 shows that this is, in fact, what we observed experimentally. The most substantial changes occur to bonds 1, 2, 7, 8, and 13, while bonds 6, 9, and 12 undergo very small, often statistically meaningless, changes. Bond 1, which represents the interpyridyl ring bond distance, shrinks substantially from 1.484(av) Å for the neutral parent compound to 1.429(3) Å for **3** and to 1.385(av) Å for **4** and **5**. Similarly, there is also a dramatic change to bond 2, which varies from 1.338(av) to 1.382(3) and 1.435(av) Å for the neutral, radical, and dianionic forms of 2,4′-bipy, respectively. For a comprehensive listing of bond distances, see Table 4. A comparison of bond distances with the theoretical values obtained from DFT calculations shows good correlations, and the same systematic trends are observable (these data are also provided in Table 4).

Table 4. Bond Lengths [Å] for 2,4′-bipy and the 2,4′-bipy$^{\bullet-}$ and 2,4′-bipy^{2-} Moieties in Species **3**−**5**[a]

		2,4′-bipy$^{\bullet-}$	2,4′-bipy^{2-}	
bond[b]	2,4′-bipy[c]	**3**	**4**	**5**
1	1.484(av) [1.489]	1.429(3) [1.431]	1.385(3) 1.384(3)	1.387(5) [1.395] 1.385(5)
2	1.338(av) [1.360]	1.382(3) [1.408]	1.430(2) 1.438(2)	1.436(4) [1.452] 1.436(4)
3	1.333(av) [1.350]	1.345(3) [1.343]	1.344(3) 1.344(2)	1.341(4) [1.334] 1.341(4)
4	1.362(av) [1.397]	1.383(3) [1.403]	1.372(3) 1.377(3)	1.377(5) [1.417] 1.376(5)
5	1.354(av) [1.398]	1.404(3) [1.422]	1.429(3) 1.427(3)	1.425(5) [1.439] 1.423(5)
6	1.370(av) [1.395]	1.371(3) [1.381]	1.353(3) 1.352(3)	1.348(5) [1.376] 1.352(5)
7	1.373(av) [1.405]	1.432(3) [1.435]	1.458(3) 1.455(3)	1.451(5) [1.461] 1.458(4)
8	1.385(av) [1.405]	1.430(3) [1.437]	1.465(3) 1.462(3)	1.467(4) [1.467] 1.471(5)
9	1.379(av) [1.395]	1.375(3) [1.384]	1.353(3) 1.360(3)	1.352(5) [1.381] 1.355(5)
10	1.325(av) [1.356]	1.360(3) [1.375]	1.388(3) 1.383(3)	1.391(4) [1.389] 1.381(4)
11	1.334(av) [1.358]	1.363(3) [1.380]	1.383(3) 1.371(3)	1.368(4) [1.400] 1.374(4)
12	1.376(av) [1.393]	1.369(3) [1.381]	1.359(3) 1.359(3)	1.370(5) [1.376] 1.358(5)
13	1.385(av) [1.406]	1.431(3) [1.436]	1.463(3) 1.467(3)	1.469(5) [1.464] 1.466(5)

[a] Data in brackets correspond to the bond lengths [Å] obtained from the optimized geometries using the computational methods described in the manuscript. [b] Bond numbering scheme, as indicated in Figure 8a. [c] Average bond metric data taken from ref 32.

Spectroscopic Characterization. A search of the chemical literature reveals a dearth of available spectroscopic information on the chemically reduced forms of 2,4′-bipyridine. While such data are readily abundant for the 2,2′-bipyridyl radical, no such reports are available for the less widely used 2,4′ isomer. Reports on the electrochemical behavior of the neutral parent compound are available,[17a] as well as a study detailing the Raman spectra of 2,4′-bipy adsorbed on an active electrode surface at various potentials.[17b] However, as with the structural data reported above, it appears that a comprehensive study of the reduced forms of this bipyridyl isomer has yet to be carried out. During the course of our research, we decided to complement the structural data that we obtained for compounds **3**−**5** with a series of EPR, IR, and Raman measurements with the aim

(32) (a) Syssa-Magalé, J.-L.; Boubekeur, K.; Palvadeau, P.; Meerschaut, A.; Schöllhorn, B. *CrystEngComm* **2005**, *7*, 302. (b) Morimoto, M.; Irie, M. *Chem.—Eur. J.* **2006**, *12*, 4275. (c) Tong, M.-L.; Ye, B.-H.; Cai, J.-W.; Chen, X.-M.; Ng, S. W. *Inorg. Chem.* **1998**, *37*, 2645.

of developing a simple diagnostic method capable of spectroscopically distinguishing between the neutral, radical, and dianonic forms of 2,4′-bipy.

Solution-phase and solid-state EPR measurements on sample **3** clearly prove the presence of a radical anion in the sample. The solution-phase spectrum displays a complicated hyperfine coupling pattern as a result of the coupling of the magnetic moment of free electron with two inequivalent ^{14}N nuclei and eight inequivalent ^{1}H atoms (a hyperfine splitting that should give rise to 2304 unique lines). The resonance is centered at a *g* value of 2.0037, which is very similar to the value of 2.0035 observed for the 2,2′-bipyrdiyl radical and comparable to that of the free electron. A nonlinear least-squares fitting of the solution-phase EPR spectrum of the 2,4′-bipyridyl radical gave coupling constant values of 6.56 and 10.10 MHz for the interaction between the electron spin and the two ^{14}N nuclei. Coupling constants for interactions with the eight inequivalent proton environments were determined to be −3.52, −2.88 −12.42, 1.28, −1.15, −6.56, −7.99, and 1.21 MHz. These values are in good agreement with the isotropic Fermi contact coupling constants determined by DFT calculations (a list assigning coupling constants for the radical anion is provided in the Supporting Information).

Similarly, a solid sample of **3** also reveals a strong resonance with a *g* value of 2.0037 with no hyperfine coupling. This symmetrical resonance is consistent with what would be expected from such a sample, and there is no evidence of the asymmetry observed for sample **1** (see the Supporting Information). As with the 2,2′-bipyridyl dianion, solid samples of **4** and **5** also give rise to very weak resonances, presumably arising from nonstoichiometric compositions of formulas $A_{4-x}(2,4'\text{-bipy}^{2-})_{2-x}$-$(2,4'\text{-bipy}^{\bullet-})_x(en)_{3.5}$ (A = K, Rb). These resonances are very weak compared to that observed for a solid sample of **3** and may arise because of the presence of trace amounts on the bipyridyl radical in the crystallographic sites occupied by the dianion.

As with the 2,2′ isomer, the IR spectrum of compound **3** reveals the presence of a unique ring deformation mode for the radical anion in the 900−1000 cm^{-1} region. This peak appears at 944 cm^{-1} for **3** and is clearly absent from the neutral parent compound. The C=C and C=N stretching region, however, is not as informative as that of the 2,2′-isomer radical. There is a stretching frequency absorption at 1559 cm^{-1} for the 2,4′-bipyridyl radical that is absent from neutral 2,4'-bipy; however, the rest of the region does not allow for a diagnostic assignment of charge. Several strong bands that are present in the IR spectrum of neutral 2,4′-bipy are absent from the spectrum of the radical anion, and these may be used as an additional diagnostic tool. These occur at 730, 773, 851, 1043, and 1066 cm^{-1} for the neutral species and are absent from the spectrum of the radical anion.

The IR spectra of compounds **4** and **5** are largely identical, as would be expected for two isomorphic species that vary in the nature of the alkali-metal cations associated with the 2,4′-bipyridyl dianions. There are marked differences between the IR spectra of these two compounds and those of their neutral and radical counterparts. Two strong absorption peaks appear in the 900−1000 cm^{-1} region that were not present in the spectrum of 2,4′-bipy and where only one strong band was observed for the 2,4′-bipyridyl radical. These occur at 900 and 950 cm^{-1} and 902 and 951 cm^{-1} for **4** and **5**, respectively. An additional pair of strong peaks corresponding to in-plane bending modes may also be observed at 1257 and 1290 cm^{-1} and 1255 and 1291 cm^{-1} for **4** and **5**, respectively. This region of the IR spectrum (between 1250 and 1300 cm^{-1}) typically shows a single weak band for the radical anion (1267 cm^{-1}) and extremely weak peaks for the neutral parent compound. As a result, it may also be used diagnostically to establish the charge associated with a 2,4′-bipyridyl moiety. The C=C and C=N stretching region reveals the presence of two strong bands for **4** and **5**, which appear at 1574 and 1607 cm^{-1} and 1576 and 1604 cm^{-1}, respectively. While these peaks cannot be employed reliably as a characteristic fingerprint, they appear to be shifted to higher wavenumbers by approximately 10 cm^{-1} compared to those observed for the radical species **3**.

The Raman spectra recorded for compounds **3**−**5** are found to be in very good agreement with the corresponding IR spectra. This is unsurprising considering the C_s point symmetry of a planar 2,4′-bipyriyl moiety, which would make all possible vibrational modes both IR- and Raman-active. The number of coincidental IR- and Raman-active modes is high, particularly for the 2,4′-bipyridyl dianions **4** and **5**, where a minimum of 12 bands common to both species were found to coincide in the IR and Raman spectra. Additional vibrational modes might also be observed to arise from the en molecules present in species **3**−**5** and from trace amounts of impurities.

4. Conclusions

During the course of these studies, we have developed a versatile methodology for the synthesis of bulk samples of compositionally pure salts of 2,2′- and 2,4′-bipyridyl radical anions and dianions, which we have characterized in compounds **1**−**5**. These studies help to elucidate some of the more obscure aspects of the chemistry of these highly reductive air- and moisture-sensitive species. The crystallographic data provided help to draw important correlations between the electronic structure and bond metric data, providing one of several diagnostic tools for the elucidation of the charge associated with partially reduced bipyridyl moieties. This area has proven contentious in the field of coordination chemistry in the past, particularly when pertaining to the assignment of the formal oxidation states of 2,2′-bipyridyl complexes of low-valent transition metals. Furthermore, the spectrochemical studies that we have carried out help to complement the existing data in the chemical literature and to provide further analytical tools with which to determine the presence of reduced forms of such prevalent ligand systems. At present, we are investigating a series of mid-row and late-transition-metal complexes of these ligand systems in which the bipyridyl moieties exhibit a large degree of negative charge on the ligand backbones, with the aim of developing "switchable" materials capable of undergoing structural changes when submitted to external stimuli.

Acknowledgment. We thank the EPSRC (EP/F00186X/1, PDRA to M.S.D.) and the University of Oxford (studentship to M.I.) for financial support of this research. We also thank Steve Boyer (London Metropolitan University) for performing all elemental analyses and the Oxford Crystallographic Service, the Oxford Supercomputing Centre, and CAESR for access to instrumentation. Special acknowledgment is also given to Dr. Jeffery Harmer for his assistance in simulating solution-phase EPR spectra.

Supporting Information Available: X-ray crystallographic file in CIF format (**1a**, **1b**, and **2**−**5**), powder X-ray diffraction patterns, crystal packing diagrams, vibrational spectroscopy data for compound **5**, a full ref 21, and EPR, IR, and Raman data. This material is available free of charge via the Internet at http://pubs.acs.org.